Solid Freeform Fabrication 2017: Proceedings of the 28th Annual International Solid Freeform Fabrication Symposium – An Additive Manufacturing Conference
Reviewed Paper

Temperature and Humidity Variation Effect on Process Behavior in Electrohydrodynamic Jet Printing of a Class of Optical Adhesives

Patrick Sammons[1], Sahit Bollineni[1], Ritika Sibal[2] Kira Barton[1]

University of Michigan, Ann Arbor, MI 48109
[1]Mechanical Engineering Department
[2]Electrical Engineering and Computer Science Department

Abstract

Electrohydrodynamic jet (e-jet) printing is an emerging additive manufacturing process that utilizes an electric field to eject material from a micro-/nano-scale microcapillary nozzle. Due to its contemporary nature and the complex physics which govern the process, little is known about printing behavior sensitivity with respect to environmental condition variability. The aim of this work is to construct a systematic experimental design to test and evaluate the relationship between two environmental variables, temperature and relative humidity, and key process metrics initiating ejection voltage, printing frequency, and diameter of material ejected. A factorial statistical design of experiments is used to investigate the parameter space. Results are used to identify temperature and humidity ranges that give robust printing regimes for a specific class of optical adhesives. Best-fit curves are determined for several of the input-output relationships, which provide a predictive model for the ink behavior.

Introduction

Electrohydrodynamic (e-jet) printing is a micro-/nano-scale additive manufacturing (AM) process which exhibits potential for numerous applications including printed electronics and sensors [1, 2] and tissue engineering structures [3]. The governing physics of e-jet printing, i.e., electrohydrodynamics, enable superior resolution (< 10 μm) and printing of inks with a wider range of rheological properties (1×10^1 to 1×10^6 cps) over similar scale processes such as ink- and aerosol-jet. Because of these properties and the inherent advantages of AM, e-jet printing spans the resolution-cost gap between ink- and aerosol-jet and traditional lithographic micro-/nano-scale manufacturing process.

In e-jet printing, an electric field is generated between an emitter carrying the to-be-printed ink and an attractor. When the electric field reaches a critical magnitude, the ink at the emitter deforms into a Taylor cone [4] and issues a jet of material directed towards the attractor. Typically, as is the case in this work, the emitter is a conductive microcapillary nozzle filled with ink and the attractor is a conductive substrate located beneath the nozzle orifice. In this situation, the material jet is capable of producing substrate-side features significantly smaller than the nozzle orifice size. Figure 1 shows a schematic of the nozzle-conductive substrate setup used in e-jet printing.

In typical operation, e-jet printing is conducted in ambient conditions. While this is advantageous in that no environmental control is needed, variations in ambient conditions can alter the printing behavior. Despite this, no apparent literature is available regarding printing behavior trends with respect to ambient conditions, in particular temperature and humidity. However, other factors influencing printing behavior, such as standoff distance and nozzle diameter, e.g. [7], have been investigated. In this work, the effects of ambient temperature and humidity on the rate

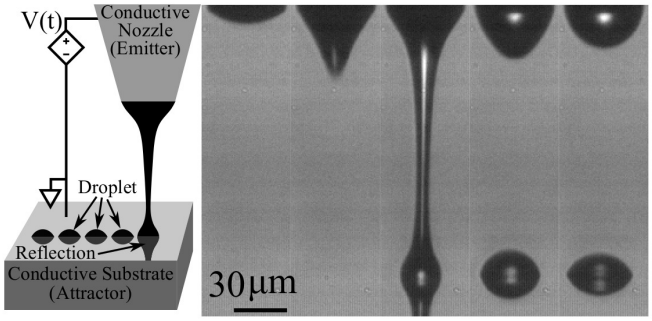

Figure 1: Schematic of e-jet printing with a microcapillary nozzle and a conductive substrate.

at which ink is jetted from the nozzle, the resulting substrate-side droplet size, and the voltage at which jetting initially occurs are investigated. The rest of this paper is structured as follows. First, a description of the hardware system used to conduct the experiments is given. Then, details regarding the experiment design are given including the independent and dependent variables of interest. This is followed by a presentation of the experiment outputs and a discussion. Finally, a summary of the work and conclusions are given.

System Description

The printer used in this work is based on a commercially available 3D printer, a Velleman K8200 3D printer. The printer has been altered to accept an e-jet print head which consists of a 3D printed nozzle holder and an additional Z-axis stage. In addition to the print head, a custom system-level controller, utilizing an Arduino Mega microcontroller, is implemented to control the stage motion (the X-, Y-, Z-, and Fine Z-axis) and the UV curing tool. The curing tool consists of a UV LED connected to the system power source and a hardware and software switch. Two other subsystems are integrated into the e-jet printer: a Trek 677B High Voltage Amplifier and a Basler acA460-750um USB camera. The Trek amplifier output is routed to the 3D printed nozzle holder and the substrate stand is grounded. The Basler USB camera is used for in-situ monitoring and initial setup of the printing process.

The e-jet printer described above is placed inside a Caron 7000-10-1 Environmental Chamber. The environmental chamber (EC) is capable of creating environmental temperatures in the range of 5 to 70 °C with control to ± 0.1 °C and relative humidity in the range of 20 to 95% with control to $\pm 2\%$. A schematic of the experimental system is shown in Figure 2, in addition to photographs of the actual system inside the environmental chamber.

Experiment Description

This section provides details regarding the experimental setup. The printing regime for all of the experimental trials is DC printing, where the voltage is held constant as the substrate is traced along a raster pattern. Two types of optical adhesive, Norland Optical Adhesive (NOA) 81 and 68, are characterized in the tests. The inks are printed from World Precision Instruments 10 μm inner diameter pre-pulled microcapillary nozzles with Luer lock connections (WPI TIP10TW1-L).

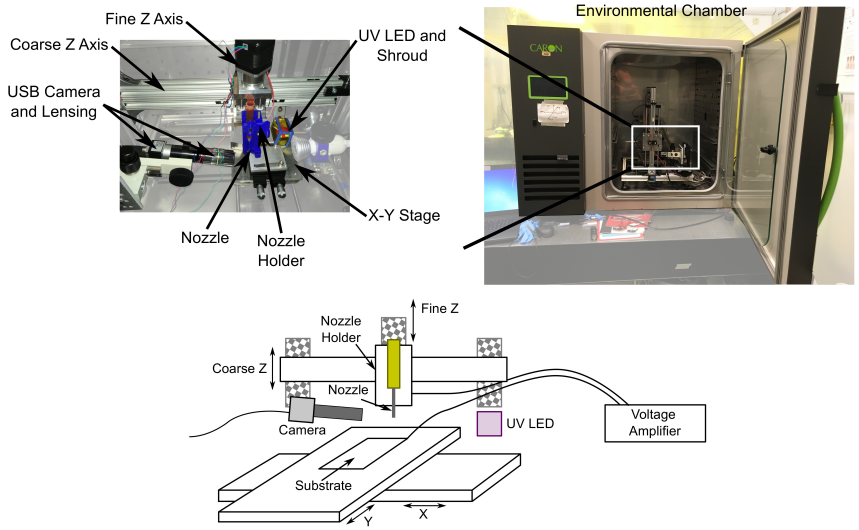

Figure 2: Photograph of the e-jet printer inside the environmental chamber and detail (top) and schematic of the e-jet printer (bottom)

These nozzles are sputtered with a palladium-gold alloy to render the glass surface conductive and a hydrophobic coating is applied to the nozzles to mitigate wetting of the nozzle surface. The substrate used in these tests are 1 inch by 3 inch indium tin oxide (ITO) coated glass microscope slides with a specified resistance of 100 Ω/in^2.

While the formulations of NOA 81 and 68 are proprietary, they are listed as mercapto-esthers. NOA 81 contains approximately 50% triallyl isocyanurate [5] with NOA 68 being comprised of approximately 75% mercapto-esther and 25% tetrahydrofurfuryl [6]. Typical viscosity properties of NOA 81 and 68 are $\mu = 3.0\times10^2$ cps and $\mu = 5.0\times10^3$ cps, respectively.

The tests here are three-level, three factor full factorial tests and as such have three factors or independent variables. Three response variables are also selected. For each level, a raster pattern is commanded on the X-Y stage. This pattern, coupled with the DC mode printing regime, results in a pattern of discrete droplets termed a dot matrix.

A. Independent Variables

Of the three factors selected for the tests, two are related to the environmental conditions and are selectable on the EC. The third factor is used to verify previously observed trends for e-jet printing. The three factors are:

1. Environmental absolute humidity χ_a (kg/m^3)
2. Environmental temperature T (K)
3. Voltage level V (V)

Absolute humidity χ_a is used to provide a temperature-independent variable for the experimental levels. However, because the EC operates in terms of relative humidity χ_r (%), the chosen AH levels are converted to RH using the definitions of relative and absolute humidity [8],

$$\chi_r = \chi_a \frac{R_v T}{e_S(T)} \tag{1}$$

where $R_v = 461.5$ J/kg-K is the gas constant for water vapor and e_S is the saturation pressure of water (Pa) as a function of absolute temperature. Saturation pressure of water as a function of temperature is found using the August-Roche-Magnus formula [9],

$$e_S(T) = a \exp\left(\frac{bT + c}{T + d}\right) \tag{2}$$

where $a = 6.1094$, $b = 17.625$, and $c = 4.814 \times 10^3$, and $d = 516.19$.

As stated above, the DC mode in e-jet printing is characterized by a constant voltage during the print. Further, because there is a minimum level at which jetting occurs, the voltage level factor is scaled by this initialization voltage V_I.

The levels chosen for each of the variable are given in Table 1. The values for absolute humidity were chosen such that, when mapped to relative humidity are suitable for operation of the stepper motors and camera inside the environmental chamber. These limits are shown in Figure 3. The levels for voltage, in addition to being scaled by the initialization voltage, are chosen such that the expected jetting frequency is slow enough that the X-Y stage is able to move sufficiently far between ejections and droplet merging does not occur.

Table 1: Independent variable levels.

Variable	Low Level	Middle Level	High Level
Absolute Humidity, χ_a (kg/m^3	4.0	6.0	7.9
Temperature, T (K) [°C]	284.9 [11.75]	296.965 [23.5]	305.4 [32.25]
Voltage, V (V)	$1.05V_I$	$1.10V_I$	$1.15V_I$

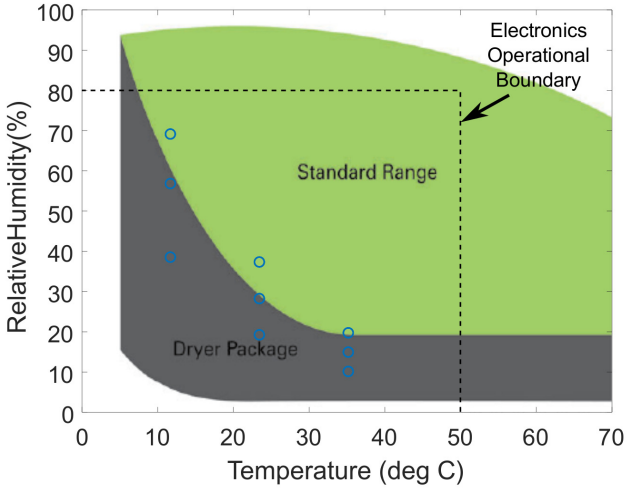

Figure 3: Environmental chamber capabilities (solid areas), electronics operational boundary, and independent variable levels (o).

B. Dependent Variables

The response/dependent variables, or metrics, for these tests are temporal droplet ejection frequency, droplet diameter, and initialization voltage. Together, jetting frequency and droplet

diameter dictate the feature size and material deposition rate in e-jet. These are extremely important for repeatable fabrication of nano-/micro-scale structures. Alternatively, initialization voltage provides a baseline value for energy consumption needed per droplet. Further, the electric field strength significantly influences the shape and behavior of the actual jet [11]. Therefore, it is important to understand how the above factors impact the voltage scaling. A schematic for describing droplet ejection, temporal frequency and initialization voltage are given in Figure 4.

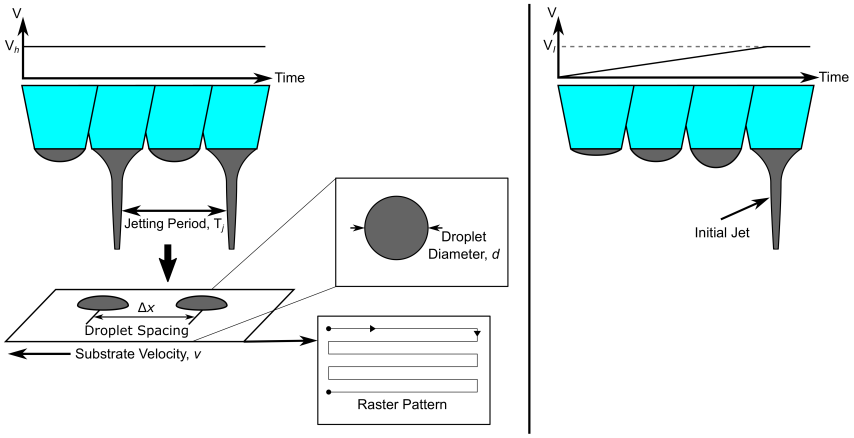

Figure 4: Schematic depicting the dependent variables for the work.

C. Printing Procedure

The experimental trials consist of two main processes: printing and analysis. In both processes, several steps are performed. The printing step is detailed here while the analysis is addressed in the following subsection. The steps detailed here and in the next subsection are presented in a flow chart in Figure 5.

1. Initialize Nozzle: As mentioned above, the emitter in this work is a conductive microcapillary nozzle. This nozzle is connected to a syringe barrel, which acts as an ink reservoir. In order to drive the ink from the barrel to the tip of the microcapillary, a small amount of pressure ($<$ 5 PSI) is needed. Therefore, the syringe barrel, with the microcapillary attached, is connected to a clean air pressure line. While the nozzle is hydrophobically coated, excess ink can wet the nozzle exterior. To minimize this effect, the nozzle is then positioned roughly 50-100 μm above the substrate and approximately 300 V are applied between the nozzle and substrate. Once ink begins to flow from the nozzle tip, air pressure and voltage are shut off. The nozzle is now considered initialized and is ready to print.
2. Environmental Chamber Setting: Referring to the experimental plan, the appropriate temperature and relative humidity set points are entered into the EC. Because the trials are randomized, some combinations of RH and temperature require long periods for the EC controller to reach the desired set point.
3. Determine Initialization Voltage: At the chosen standoff distance, which here is set to 93.75 μm and corresponds to 75 pixels in the system camera, the voltage output from the amplifier is manually increased until a jet of material is observed to issue from the nozzle. The voltage at which this initial jet is observed is termed the initial jetting voltage as shown schematically in Figure 4.

4. Print Marker Droplets: The only in-situ observation of the printing process is high-magnification video centered on the nozzle. Thus, it is difficult to ascertain, post-printing, which set of parameters corresponds to a particular dot matrix. Therefore, a dot pattern is printed at the beginning of each dot matrix to ensure proper correspondence between printing behavior and independent variable set.
5. Print Raster: The printing of the ink at the particular set of independent variables is conducted in a raster pattern of 3 forward-reverse pairs, schematically shown in Figure 4. The resulting pattern is termed a dot matrix.
6. Cure: In order to preserve the droplet morphology on the glass substrate while printing at different environmental conditions and during transport between the printer and the optical microscope, a UV LED is used to cure the printed ink. After each raster, the substrate is shuttled to the UV LED, shrouded in UV opaque plastic to protect the ink still inside the nozzle from the curing mechanism, and the LED is turned on for 60 seconds. The LED is then turned off and the substrate is returned to the printing location.

The steps detailed above are iterated three times for each independent variable set. After an entire glass slide has been filled with printed raster patterns, the slide is removed and processing begins for those variable sets on the slide.

D. Data Processing Procedure

In order to characterize the printing behavior for each variable set, optical micrographs are taken. Here, an Olympus BX43 Optical Microscope equipped with a 20X objective is used to image the printed droplets. The chosen objective is a balance between resolution (enough pixel information for each droplet) and field of view (large number of droplets are still visible). The processing steps are detailed below and outlined in the flowchart schematic shown in Figure 5. The image processing steps described below are carried out in ImageJ [10], unless otherwise noted.

1. Microscope Images: As mentioned above, each raster is imaged with a 20x objective. Because it is not possible to image the entire raster pattern in a single image, several images for each pattern are required. The microscope stages are jogged and an image of each section of the raster is recorded. These images are not stitched together.
2. Image Conversion: The optical microscope natively captures images in full color. In order to perform the subsequent image processing steps, the image must be converted to an 8-bit image. This conversion can be performed automatically in ImageJ.
3. Adjust Circularity and Threshold: The final product of the image processing steps is a list of circle centers and areas that correspond to the printed droplets. In order to effectively identify the droplets, thresholds are set for both the circularity of the identified shapes and the area. Further, in order to remove image artifacts not associated with the droplets, a threshold is applied to the image such that only those channels associated with the droplets remain.
4. Perimeter and Center Locations: The perimeter and centroid of the shape identified as a droplet is calculated and reported. This data is imported to MATLAB to conduct the final step in processing.
5. MATLAB Processing: The centroid data is sorted such that spatially adjacent droplets are ordered consecutively in a storage vector. Difference methods are used to calculate the incremental distance between centroids. Using this data and the known stage speed, jetting

frequency is calculated as

$$f = \frac{v}{\Delta x} \tag{3}$$

where f is the average jetting frequency (Hz), v is the substrate speed (μm/s), and Δx (μm) is the measured distance between adjacent droplet centroids. The droplet is assumed to be circular and thus the diameter is calculated from the measured perimeter as,

$$d = \frac{P}{\pi} \tag{4}$$

where d is the droplet diameter (μm) and P is the droplet perimeter (μm).

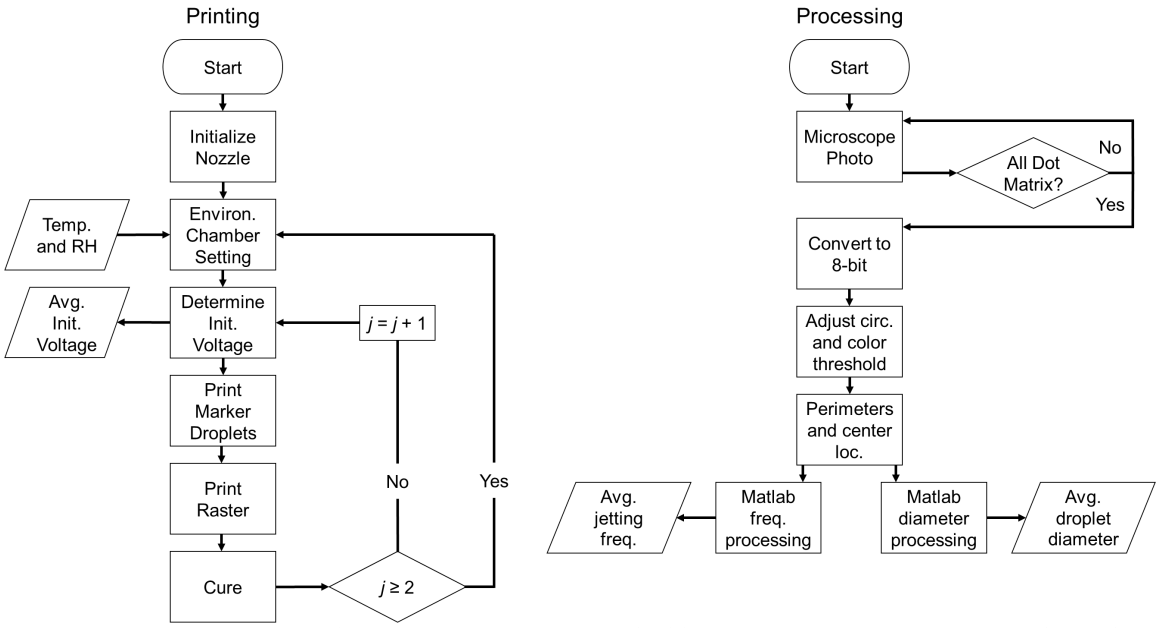

Figure 5: Flow chart of the printing process (left) and the analysis process (right).

Results and Discussion

Following the steps outlined above, data is prepared for both inks: Norland Optical Adhesive 81 and 68. In the first subsection here, data is presented regarding correlations between temperature, humidity, and voltage and jetting frequency and droplet diameter for both inks. Correlations between temperature and humidity and initial jetting voltage are also given. In the second subsection, general trends between the two inks are discussed.

E. Ink Characterization

Tables 2 and 3 give the correlation coefficients between the independent variable and the dependent variables, as applicable, using MATLAB's `corr`. Positive correlations are observed for temperature and absolute humidity with respect to diameter and voltage with respect to frequency. Negative correlations are observed between temperature and absolute humidity with respect to frequency and initial jetting voltage and between voltage and diameter. Plots of the data and the

correlation line for coefficients above magnitude 0.5 are shown in Figures 6 through 8. In each figure, the error bars represent one standard deviation from the mean value for each response variable at each experimental set point and provide a measure of uncertainty.

Table 2: Correlation Coefficients for NOA 81.

	Response Variable		
Factor Variable	**Diameter**	**Frequency**	**Init. Jet. Voltage**
Temperature	0.69	-0.51	-0.96
Abs. Humidity	0.23	-0.05	-0.04
Voltage	-0.63	0.56	N/A

Table 3: Correlation Coefficients for NOA 68.

	Response Variable		
Factor Variable	**Diameter**	**Frequency**	**Init. Jet. Voltage**
Temperature	0.93	-0.88	-1.0
Abs. Humidity	0.24	-0.13	-0.01
Voltage	-0.90	0.68	N/A

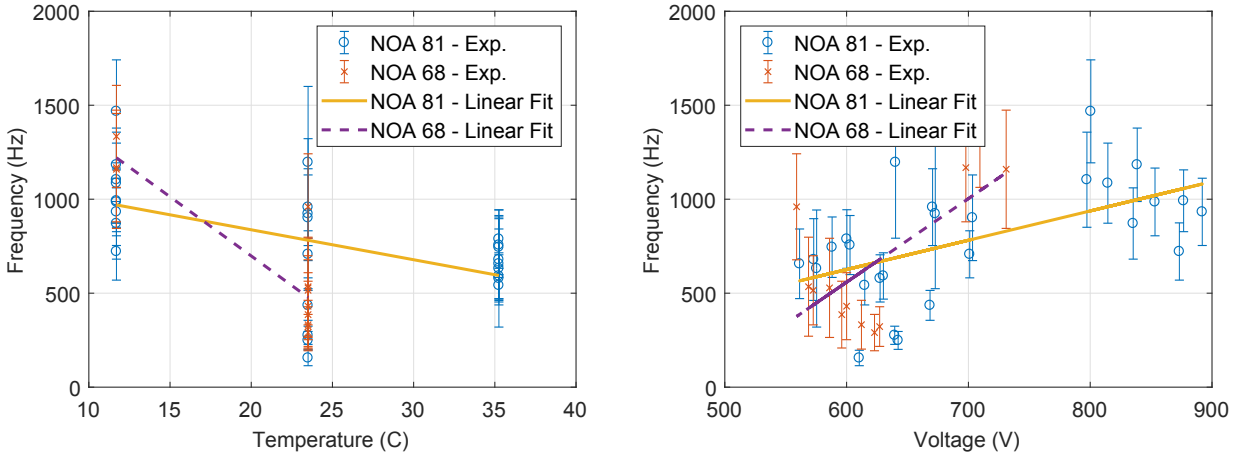

Figure 6: Mean jetting frequency as a function of temperature (left) and voltage (right) for NOA 81.

F. Printing Regimes and Ink Comparison

Examining the relationships presented above yields insight into selecting a suitable regime for printing, given a specific environmental condition. As stated above and supported by the correlation coefficients, absolute humidity does not appear to have a significant impact on printing behavior. However, temperature and voltage levels can have large impacts on printing behavior. The voltage trends presented above agree with previously published scaling laws that illustrate the positive correlation between voltage and frequency [7], as well as the negative correlation between that factor and droplet diameter.

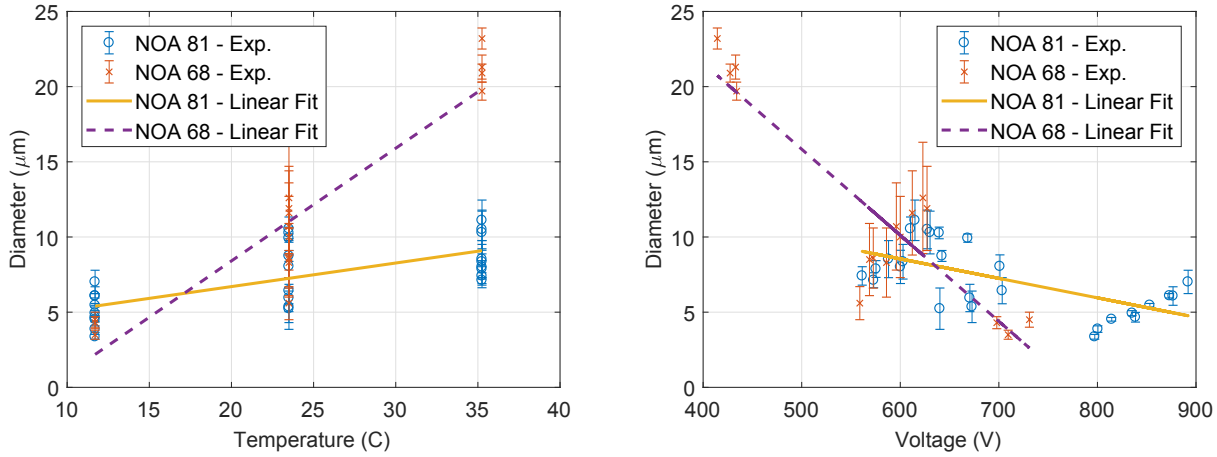

Figure 7: Mean droplet diameter as a function of temperature (left) and voltage (right) for NOA 81 and 68.

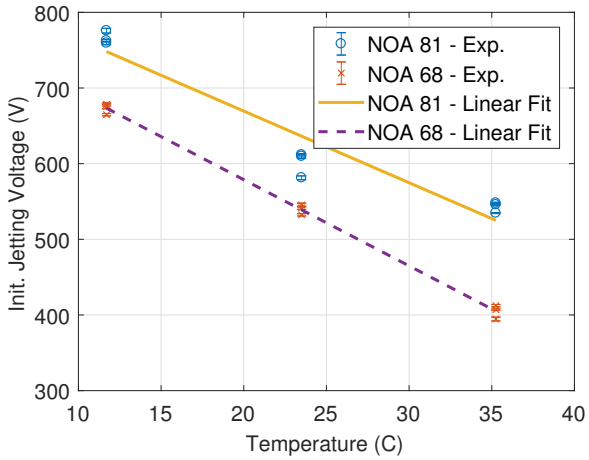

Figure 8: Mean initial jetting voltage as a function of temperature for NOA 81 and 68.

From Figure 6, it can be observed that droplet diameter is significantly influenced by voltage and temperature. While the voltage behavior follows that of existing scaling laws [7], the temperature trend reveals a previously unreported trend. For NOA 81, variations of 10 °C can lead to an approximately 2 μm change in diameter. This effect is amplified for NOA 68. This could result in a significant problem when trying to reproduce printed structures at different points throughout a calendar year when room temperature can vary significantly depending on outside temperatures and building HVAC set points. In addition to the trend seen for diameter in Figure 6, a negative correlation between temperature and frequency and temperature and initial jetting voltage can be observed in Figures 7 and 8, respectively. Comparing the two tested inks indicates that NOA 68 is more sensitive to the tested inputs. For each of the relationships shown in Figures 6 through 8, NOA 68 shows a higher correlation coefficient than NOA 81.

While not a complete exploration of the parameter space, the results presented here represent an initial characterization of the impact of environmental conditions on e-jet printing. Future studies will include a wider range of materials which may reveal similar trends as those shown

here, in addition to possibly stronger correlations with humidity.

Conclusion

E-jet printing is an advanced manufacturing process which is capable of producing nano-/micro-scale features with materials which have a wide range of material properties. While general printing behavior trends are observed with respect to nozzle diameter and voltage in literature, little is known about the influence of ambient conditions on the printing behavior.

Here, a series of experiments were conducted to determine the effects of temperature, humidity, and voltage on the droplet diameter, jetting frequency, and initial jetting voltage for a class of optical adhesives. The independent parameters (temperature, humidity, and voltage) were chosen such that they were feasible given hardware constraints and did not affect electronics in the case of humidity. While limited by some constraints, the selected values represent a range that may be observed in a lab over the course of a calendar year. The identified relationships revealed both known trends and previously unobserved behavior. Correlations between voltage and diameter and frequency help validate the printing behavior observed with respect to temperature and humidity. For the class of materials considered here, humidity did not appear to be highly correlated with any of the selected process metrics, while temperature correlated significantly with diameter, frequency, and initial jetting voltage. These identified trends are important for process planning. Future investigations will consider other classes of materials which may reveal dependence on ambient humidity.

References

[1] Jeong, S., et. al., 2013, "Air-Stable Surface-Oxide Free Cu Nanoparticles for Highly Conductive Cu Ink and Their Application to Printed Graphene Transistors," *Journal of Materials Chemistry C*, vol. 1, pp. 2704-2710.

[2] Park, J.-U., et. al., 2008, "Nanoscale Patterns of Oligonucleotides Formed by Electrohydrodynamic Jet Printing with Applications in Biosensing and Nanomaterials Assembly," *Nano Letters*, vol. 12, pp. 4210-4216.

[3] Wu, Y., et. al., 2017, "Direct E-Jet Printing of Three-Dimensional Fibrous Scaffold for Tendon Tissue Engineering," *Journal of Biomedical Materials and Research: Part B*, vol. 105, pp. 616-627.

[4] Park, J.-U., et. al., 2007, "High-Resolution Electrohydrodynamic Jet Printing," *Nature Materials*, vol 6, pp. 782-789.

[5] NOA 81 Material Safety Data Sheet, www.norlandprod.com/msds/noa%2081msd.html

[6] NOA 68 Material Safety Data Sheet, www.norlandprod.com/msds/noa%2068msd.html.

[7] Choi, H.K., et. al., 2008, "Scaling Laws for Jet Pulsations Associated with High-Resolution Electrohydrodynamic Printing," *Applied Physics Letters*, vol. 92, pp. 123109:1-3.

[8] Parish, O.O., Putnam, T.W., 1977, "Equations for the Determination of Humidity from Dewpoint and Psychrometric Data," NASA Technical Note.

[9] Alduchov, O.A., Eskridge, R.E., 1996, "Improved Magnus Form Approximation of Saturation Vapor Pressure," *Journal of Applied Meteorology*, vol. 35, pp. 601-609.

[10] Schneider, C.A., Rasband, W.S., Eliceiri, K.W., 2012, "NIH Image to ImageJ: 25 years of Image Analysis," *Nature Methods*, vol. 9, pp. 671-675.

[11] Lee, A., et. al., 2013, "Optimization of Experimental Parameters to Determine the Jetting Regimes in Electrohydrodynamic Printing," *Langmuir*, vol. 29, pp. 13630-13639.